IMPACT DAMAGE IN COMPOSITE STRUCTURES MANUFACTURED USING RESIN INFUSION UNDER FLEXIBLE TOOLING (RIFT) PROCESS

Mauricio V. Donadon, John M. Hodgkinson, Brian G. Falzon and Lorenzo Iannucci

Department of Aeronautics, Imperial College London, South Kensington, London, SW7 2AZ, U.K.

ABSTRACT

This paper addresses the modelling of low velocity impact behaviour of composite plates manufactured using the RIFT process. The material system investigated consists of a hybrid plain-weave fabric. A 3-D micromechanical model based on the Classical Laminate Theory (CLT) has been developed and used in conjunction with an in-plane energy based damage model which enables the degradation of the in-plane mechanical properties and the control of the energy dissipation associated with the in-plane failure mode within the Representative Volume Element (RVE) during the impact event. The material model has been implemented into the LS-DYNA3D explicit finite element code within solid elements.

1. INTRODUCTION

In recent years, a considerable effort in the aerospace industry has been dedicated towards the reduction of costs and timescales associated with composite manufacturing. Also, there is a clear need for the investigation of new fabric architectures and resin systems for improvement of the interlaminar properties, particularly under impact loading. In this context, resin infusion technologies offer significant cost advantages over the normal pre-preg route to manufacture composite aerostructures. There are no costs associated with material storage, since the fabrics used in these processes are dry. Also, high volume fraction laminates can be obtained with low void content and large structures can be produced in one operation.

Most of the work reported in the recent literature has focused on the manufacturing aspects of the RIFT process, with little published work addressing final product properties, or predictive modelling of mechanical behaviour under different loading conditions.

In this context, this paper addresses the modelling of low velocity impact behaviour of composite plates manufactured using the RIFT process. The material system investigated consists of a hybrid plain-weave fabric. A 3-D micromechanical model based on the Classical Laminate Theory (CLT) [1] has been developed and used in conjunction with an in-plane energy based damage model [2, 3] which enables the degradation of the in-plane mechanical properties and the control of the energy dissipation associated with the in-plane failure mode within the Representative Volume Element (RVE) during the impact event. The material model has been implemented into the LS-DYNA3D explicit finite element code within solid elements. The numerical predictions have been compared with experimental results for validating the proposed methodology. Technical details associated with the setting up of the RIFT facility are also presented.

2. MATERIALS AND EXPERIMENTAL METHODS

2.1 *Materials, manufacturing process and specimens dimensions:*

The fabric used in this work consists of a carbon UD non-crimp tape, which has a plain-weave pattern. The material in the warp and weft directions are T700-12K-50C carbon fibre and PPG EC09 34*2 S150 1383 glass fibre, respectively. The resin system used for manufacturing the composite plates using the RIFT process is PRIME^{TM} 20 LV epoxy infusion system [4], which has a very low viscosity allowing infusions to be carried out at room temperature (25 °C). The constituent property data used are given in Tables 1 and 2, respectively. This data was taken from various literature sources [5-8].

Table 1. Mechanical properties for the fibres.

Fibre[1]	E_{11} (GPa)	E_{22} (GPa)	G_{12} (GPa)	G_{23} (GPa)	ν_{12}	ν_{23}
T700 (carbon)	232.00	23.10	8.96	8.27	0.20	0.40
PPG EC09 (Glass)[2]	72.40	72.40	29.67	29.67	0.22	0.22

(1) Fibre assumed to be transversely isotropic, $G_{23}=E_2/2(1+\nu_{23})$
(2) Glass fibre assumed to be isotropic

Table 2. Mechanical properties for the matrix.

Matrix[1]	E_{11} (GPa)	E_{22} (GPa)	G_{12} (GPa)	G_{23} (Gpa)	ν_{12}	ν_{23}
PRIME^{TM} 20LV	2.97	2.97	1.08	1.08	0.38	0.38

(1) Matrix assumed to be isotropic, $G=E/2(1+\nu)$

The composite plates were manufactured according to the RIFT setup shown in Fig. 1.

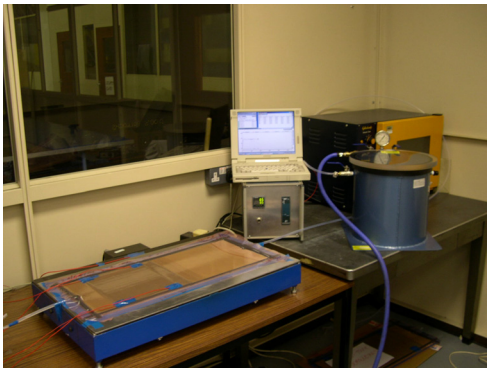

Fig. 1. RIFT setup.

Despite the flexibility of the RIFT process for manufacturing complex shapes, all the plates manufactured and tested in this work were intended to be flat. The preform stack consists of 250x250x3.6 mm^3 dry fabric plies laid up to the required stacking sequence. The manufactured and tested plates have a cross-ply lay-up of $[(0/90)_2]_s$ giving a nominal plate thickness of 3.6 mm. A flat 700x400x4 mm^3 aluminium plate was used as a mould tool. Prior to laying up the fabric, the aluminium plate was covered with a melanex film and one layer of peel ply, which aids the removal of the composite plate after cure. The fabric was then covered with a flow distribution medium on the upper and lower surfaces, in order to ensure complete fabric wetting-out. The resin flow medium was intentionally cut 30 mm short from the end of the preform near the vacuum vent to reduce the resin infusion rate within the infusion stack. Subsequently, the stack was bagged and placed on the hot platen. Next, vacuum drop tests were undertaken using a dial gauge connected to the degassing chamber. The vacuum drop test was conducted by application of full vacuum into the infusion stack and then closing the manual valve to the vacuum pump. The vacuum gauge was monitored for 30 minutes for all plates and no vacuum drop was observed. This procedure ensures the vacuum integrity within the RIFT system, which is possibly the most important manufacturing parameter for the RIFT process. The infusions were carried out at the room temperature (25 °C) and the plates were cured for 7 hours at 65 °C. The temperature variation of the laminate during the curing stage was measured by attaching thermocouples on the upper surface of the stack. The temperature measurements were taken from five different positions, four of them were placed in each corner of the square plate and the fifth being in the centre of the plate. The temperatures were recorded by means of a temperature data-logger connected to acquisition software. The point-to-point temperature variation was within +/-5 °C.

The specimen dimensions for the impact tests were based on the Boeing Test Standard [9]. The plates tested have a cross-ply lay-up of $[(0,90)_2]_s$ giving the nominal plate thickness of 3.6 mm. The dimensions of the plates were 102 mm by 152 mm.

2.2 *Test rig and data acquisition:*

Impact tests were carried out using the drop-test rig facility available in the Department of Aeronautics at Imperial College London. Different impact energy levels can be set by adjusting the drop height and impactor mass. A standard hemispherical impactor [9] with 15.75 mm in diameter was used. The impact force was measured by means of four active strain gauges mounted on the load cell cylinder above the impactor nose. The incidence velocity of the impactor was measured by means of a ruled grid attached to the impactor side and which passes a photo-emitter/photo-diode device mounted on the fixed channel guides to give a pulse form of output every time a dark line is crossed. Knowing the spacing of the grid lines and time for each to pass, the velocity can be calculated before and after the impact event. A transient data recorder recorded the experimental data. The impactor velocity and the contact force were recorded.

3. IN-PLANE FAILURE METHODOLOGY

The in-plane failure methodology proposed in this paper is schematically described in Fig. 3. The modelling is divided into two parts. The first part consists of a linear elastic analysis from which the elastic constants for the laminate are determined using a 3-D micromechanical model. In order to degrade the in-plane macromechanical elastic constants an in-plane damage model based on the Continuum Damage Mechanics (CDM) is presented.

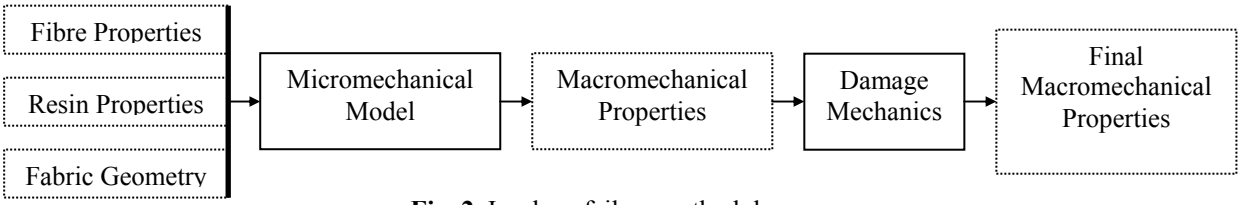

Fig. 2. In-plane failure methodology.

3.1 3-D Micromechanical Model

The homogenised mechanical behaviour requires the definition of a characteristic Representative Volume Element (RVE), which is defined as a small periodic substructure of the fabric, a geometric description of the fabric architecture and the properties of each constituent are required within the RVE. The fabric architecture is shown in Fig. 3. The 3-D micromechanical model proposed here is an extension of the 2-D model proposed by Naik and Shembekar [10].

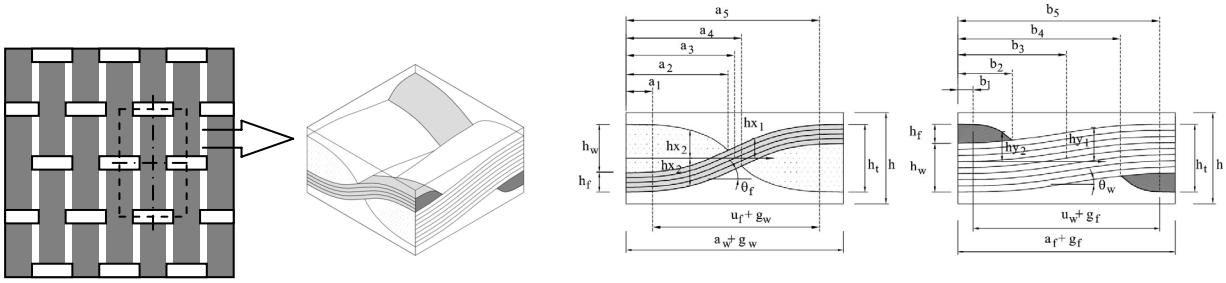

Fig. 3. RVE geometry.

Shape functions initially proposed by Naik and Shembekar [10] were used in order to describe the geometry of the unit cell. According to the authors the shape function in the warp and weft directions respectively, are given by

Warp-direction:

$0 \le y \le b_1$

$$hy_1(y) = \frac{h_t}{2} - h_f$$
$$hy_2(y) = \frac{h_t}{2} \tag{1}$$

$b_1 \le y \le b_5$

$$hy_1(y) = \left[1 + sin\left\{(y - b_3)\frac{\pi}{(u_w + g_f)}\right\}\right]\frac{h_f}{2} + \frac{h_t}{2} - h_f \tag{2}$$

$b_1 \le y \le b_2$

$$hy_2(y) = \left[\frac{h_t}{2} - hy_1(b_2)\right]cos\left\{(y - b_1)\frac{\pi}{u_w}\right\} + hy_1(b_2) \tag{3}$$

$b_4 \le y \le b_5$

$$hy_2(y) = -\left[\frac{h_t}{2} - hy_1(b_2)\right]cos\left\{(y - b_5)\frac{\pi}{u_w}\right\} - hy_1(b_2) \tag{4}$$

$b_5 \le y \le (a_f + g_f)$

$$hy_1(y) = \frac{h_t}{2}$$
$$hy_2(y) = -\frac{h_t}{2} \tag{5}$$

It has been noticed that the shape functions in the weft direction proposed by Naik and Shembekar are inconsistent with the definition of the unit cell, therefore modified shape functions for the weft direction are proposed in this work and they are given as follows,

Weft-direction:

$a_3 \le x \le a_5$

$$hx_1(x,y) = \left[1 + sin\left\{(x - a_3)\frac{\pi}{u_f + g_w}\right\}\right]\left(\frac{hy_2(y) + hy_1(y)}{2}\right) - hy_1(y)$$
$$hx_3(x,y) = -\left[1 - sin\left\{(x - a_3)\frac{\pi}{u_f + g_w}\right\}\right]\left(\frac{hy_2(y) + hy_1(y)}{2}\right) - hy_1(y) \tag{6}$$

$a_4 \le x \le a_5$

$$hx_2(x,y) = -\left[h_w - hy_1(y) + hx_3(a_4,y)\right]cos\left\{(x - a_5)\frac{\pi}{u_f}\right\} + hx_3(a_4,y) \tag{7}$$

The geometric parameters are given by

$$a_1 = \frac{a_w - u_f}{2},\ a_2 = \frac{a_w}{2},\ a_3 = \frac{a_w + g_w}{2},\ a_4 = \frac{a_w}{2} + g_w,\ a_5 = \frac{a_w + u_f}{2} + g_w \tag{8}$$

$$b_1 = \frac{a_f - u_w}{2},\ b_2 = \frac{a_f}{2},\ b_3 = \frac{a_f + g_f}{2},\ b_4 = \frac{a_f}{2} + g_f,\ b_5 = \frac{a_f + u_w}{2} + g_f \tag{9}$$

The local angles between the warp and weft yarns in a global coordinate system are respectively,

$$\theta_f(x,y) = tan^{-1}\left(\frac{dhx_1(x,y)}{dx}\right), \quad \theta_w(y) = tan^{-1}\left(\frac{dhy_1(y)}{dy}\right) \tag{10}$$

Once the fabric geometry is defined, Classical Laminate Theory (CLT) [1] can be applied for each infinitesimal section of the unit cell to determine the effective material parameters. The extensional stiffness terms are averaged within the unit cell by using the Series-Parallel model proposed by Naik and Shembekar [10]. According to their model the averaged extensional stiffness along the x-direction is written as,

$$\bar{a}_{ij}^{s}(y) = \frac{1}{a_w + g_w}\int_0^{a_w+g_w} \overline{A}_{ij}(x,y)dx \tag{11}$$

the coefficients $\bar{a}_{ij}^{s}(y)$ are then inverted to yield $\overline{A}_{ij}^{s}(y)$. In turn, these are averaged across the y-direction as follows,

$$\overline{A}_{ij}^{sp} = \frac{1}{a_f + g_f}\int_0^{a_f+g_f} \overline{A}_{ij}^{s}(y)dy \tag{12}$$

Here $\overline{A}_{ij}^{sp}$ matrix represents the average in-plane compliance constants of the lamina. In order to obtain the effective elastic constants of the lamina the $\overline{A}_{ij}^{sp}$ matrix has to be inverted and used in conjunction with equations shown below [1],

$$\begin{aligned}
E_x &= \frac{1}{\bar{a}_{11}h}, & E_y &= \frac{1}{\bar{a}_{22}h}, & E_z &= \frac{1}{\bar{a}_{33}h} \\
G_{xy} &= \frac{1}{\bar{a}_{66}h}, & G_{zx} &= \frac{1}{\bar{a}_{55}h}, & G_{yz} &= \frac{1}{\bar{a}_{44}h} \\
\upsilon_{xy} &= -\frac{\bar{a}_{12}}{\bar{a}_{11}}, & \upsilon_{xz} &= -\frac{\bar{a}_{13}}{\bar{a}_{11}}, & \upsilon_{yz} &= -\frac{\bar{a}_{23}}{\bar{a}_{22}}
\end{aligned} \tag{13}$$

3.2 Damage Model Formulation

The in-plane damage model proposed here is based on the continuum damage mechanics (CDM) approach. The methodology adopted here is based on the work proposed by Ianucci et al [2, 3]. Cracks are assumed to be smeared over the Representative Volume Element (RVE) and three effective internal variables are introduced to quantify the relative size of cracks in the cross-sectional area of the RVE, two associated with tensile behaviour in the fill and warp directions and one extra internal variable to account for the in-plane shear damage effects.

The principle of the strain equivalence [11] states that a damaged material under the nominal stress σ shows the same stress strain response as comparable undamaged material under the effective stress $\bar{\sigma}$. For a three-dimensional stress state, the relationship between effective stress and nominal stress in a local coordinate system can be expressed using a compact notation as

$$\{\sigma\} = [D(d_{11}, d_{22}, d_{12})]\{\bar{\sigma}\} \tag{14}$$

where $[D(d_{11}, d_{22}, d_{12})]$ is defined as damage matrix which contains the damage parameters associated with each particular in-plane failure mode. The compliance for orthotropic elasticity in a local coordinate system can be written in terms of the effective stresses as follows,

$$\{\varepsilon\} = [C]\{\bar{\sigma}\} \tag{15}$$

By combining the equations above the stress-strain relationship at ply level can be written as

$$\{\sigma\} = \left([C].[D(d_{11}, d_{22}, d_{12})]\right)^{-1}\{\varepsilon\} \tag{16}$$

Therefore, the stress-strain relationship at a ply level can be written in the incremental form as it follows,

$$\{\Delta\sigma\} = [E]\{[d]\{\Delta\varepsilon\} - [\Delta d]\{\varepsilon\}\} \tag{17}$$

where:

$$[E] = \frac{1}{\gamma}\begin{bmatrix} E_{11}(1-\nu_{23}\nu_{32}) & E_{22}(\nu_{12}+\nu_{32}\nu_{13}) & E_{33}(\nu_{13}+\nu_{12}\nu_{23}) & 0 & 0 & 0 \\ E_{11}(\nu_{21}-\nu_{31}\nu_{23}) & E_{22}(1-\nu_{13}\nu_{31}) & E_{33}(\nu_{23}+\nu_{21}\nu_{13}) & 0 & 0 & 0 \\ E_{11}(\nu_{31}-\nu_{21}\nu_{32}) & E_{22}(\nu_{32}-\nu_{12}\nu_{31}) & E_{33} & 0 & 0 & 0 \\ 0 & 0 & 0 & G_{23} & 0 & 0 \\ 0 & 0 & 0 & 0 & G_{31} & 0 \\ 0 & 0 & 0 & 0 & 0 & G_{12} \end{bmatrix}$$

$$[d] = \begin{bmatrix} (1-d_{11}) & 0 & 0 & 0 & 0 & 0 \\ 0 & (1-d_{22}) & 0 & 0 & 0 & 0 \\ 0 & 0 & 1 & 0 & 0 & 0 \\ 0 & 0 & 0 & 1 & 0 & 0 \\ 0 & 0 & 0 & 0 & 1 & 0 \\ 0 & 0 & 0 & 0 & 0 & (1-d_{12}) \end{bmatrix} \quad [\Delta d] = \begin{bmatrix} \Delta d_{11} & 0 & 0 & 0 & 0 & 0 \\ 0 & \Delta d_{22} & 0 & 0 & 0 & 0 \\ 0 & 0 & 0 & 0 & 0 & 0 \\ 0 & 0 & 0 & 0 & 0 & 0 \\ 0 & 0 & 0 & 0 & 0 & 0 \\ 0 & 0 & 0 & 0 & 0 & \Delta d_{12} \end{bmatrix}$$

$$\gamma = 1 - \nu_{12}\nu_{21} - \nu_{23}\nu_{32} - \nu_{31}\nu_{13} - 2\nu_{21}\nu_{32}\nu_{13}\,.$$

The Poisson's ratio must be reduced in a similar manner to the Young's module to maintain the positive definiteness of the material stress-strain law, therefore

$$\frac{\nu_{ij}(1-d_{ii})}{E_{ii}(1-d_{ii})} = \frac{\nu_{ji}(1-d_{jj})}{E_{jj}(1-d_{jj})} \tag{18}$$

The associated elastic strain energy at a given stage of damage is given as,

$$W(d_{11}, d_{22}, d_{12}) = \frac{1}{2}\sigma^T\varepsilon \tag{19}$$

Therefore, the *thermodynamic forces* associated with each failure mode can be derived as follows,

$$\begin{aligned} Y_{11} &= \frac{\partial W}{\partial d_{11}} = \frac{1}{2}\frac{\sigma_{11}}{E_{11}(1-d_{11})^2} \\ Y_{22} &= \frac{\partial W}{\partial d_{22}} = \frac{1}{2}\frac{\sigma_{22}}{E_{22}(1-d_{22})^2} \\ Y_{12} &= \frac{\partial W}{\partial d_{12}} = \frac{1}{2}\frac{\sigma_{12}}{G_{12}(1-d_{12})^2} \end{aligned} \tag{20}$$

In continuum damage mechanics the variables Y_{ij} have a meaning of energy released per unit of volume due to the advancement of damage [11].

The increment of work dissipated for an increase in the damage can be obtained from Eq. (20) as follows,

$$\Delta W_{ij} = Y_{ij}\Delta d_{ij} \tag{21}$$

Assuming damage is an irreversible local process, the material behaviour cannot violate the first and second thermodynamic laws, therefore the following dissipation inequality arises [12],

$$W_{ij}\dot{d}_{ij} \geq 0 \tag{22}$$

where $\dot{d}_{ij}$ is the damage rate. Such restriction means that the energy dissipated associated with a particular damage mode must be always positive throughout the damage process.

The criteria for damage initiation in tension for the warp, weft and inplane shear are defined in terms of the strain and they are given by

$$\begin{aligned} g_{11} &= \left(\frac{\varepsilon_{11}}{\varepsilon_{11}^{0}}\right)^{2} + \left(\frac{\varepsilon_{12}}{\varepsilon_{12}^{0}}\right)^{2} - 1 = 0 \\ g_{22} &= \left(\frac{\varepsilon_{22}}{\varepsilon_{22}^{0}}\right)^{2} + \left(\frac{\varepsilon_{12}}{\varepsilon_{12}^{0}}\right)^{2} - 1 = 0 \\ g_{12} &= \left(\frac{\varepsilon_{12}}{\varepsilon_{12}^{0}}\right)^{2} - 1 = 0 \end{aligned} \tag{23}$$

where ε_{ij}^{0} correspond to the strain threshold at which damage starts for each failure mode. The selection of a damage growth law for a particular failure mode depends on the composite material system and it controls the amount of dissipated energy associated with the damage process. The damage evolution laws adopted here are based on strain and their general form are given in an incremental form as follows,

$$\Delta d_{11} = \frac{\varepsilon_{11}^{f}}{\varepsilon_{11}^{f} - \varepsilon_{11}^{0}}\left[\frac{\varepsilon_{11}^{0}}{\varepsilon_{11}^{2}}\right]\Delta\varepsilon_{11} \tag{24}$$

$$\Delta d_{22} = \frac{\varepsilon_{22}^{f}}{\varepsilon_{22}^{f} - \varepsilon_{22}^{0}}\left[\frac{\varepsilon_{22}^{0}}{\varepsilon_{22}^{2}}\right]\Delta\varepsilon_{11} \tag{25}$$

$$\Delta d_{12} = n\alpha\left[\frac{\varepsilon_{12}}{\varepsilon_{12}^{0}}\right]^{n-1}\Delta\varepsilon_{12} \tag{26}$$

where the constants ε_{ij}^{f}, α and n control the damage nucleation and energy dissipated during the damage process.

4. FINITE ELEMENT MODEL

The finite element model consists of a 102x152x3.6 mm^3 rectangular composite plate with clamped edges impacted by a steel hemispherical impactor under an impact energy of 20 Joules. The mass and diameter of the hemispherical projectile are 2.7 Kg and 15.75 mm, respectively. The composite plate has a cross-ply $[(0/90)_2]_s$ lay-up. The macromechanical properties for each composite layer were predicted using the 3-D macromechanical model presented before. The impactor was assumed to be rigid and the plate was modelled using solid elements with a single integration point available in LS-DYNA [13]. Automatic surface-to-surface contact logic, which is based on the Hertzian contact law, was used to model the contact between the impactor and the composite plate. The laminate was modelled using one solid element per layer through the thickness. The finite element mesh was generated using the INGRID pre-processor [14] and the results were visualised using LS-PRE/POST [15]. The material model proposed has been implemented as a user-defined material *umat42v*. The

damage variables were stored and an effective damage variable (d^{ef}=max (d_{11}, d_{22}, d_{12}) = 1.0) was defined for deleting the damaged elements using the erosion algorithm available in LS-DYNA. The FE mesh is shown in Fig. 4.

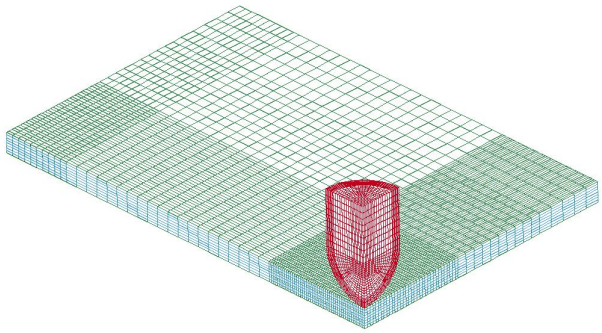

Fig. 4. FE mesh.

5. RESULTS & DISCUSSION

The elastic macromechanical properties for the fabric were predicted using the proposed micromechanical model. The geometric parameters were measured using a optical microscope, with an amplification of 25x and their values are presented in Tab. 3.

Table 3. Geometric parameters for the micromechanical model

a_f (μm)	a_w (μm)	h_f (μm)	h_w (μm)	h_t (μm)	h (μm)	g_f (μm)	g_w (μm)	u_f (μm)	u_w (μm)
1112	2350	116	329	445	445	4900	60	1568	232

Due to the complexity of the shape functions used for the geometrical modelling of the fabric, a numerical integration procedure based on the trapezoidal rule has been used for obtaining the macromechanical properties. The properties for the carbon fibre, glass fibre and resin were taken from Tables 1 and 2, respectively. The predictions for the macromechanical properties are given in Table 4.

Table 4. Predictions for the macromechanical properties

E_{11} (GPa)	E_{22} (Gpa)	E_{33} (Gpa)	G_{12} (Gpa)	G_{13}=G_{23} (Gpa)	ν_{12}	ν_{13}=ν_{23}
116.64	12.33	14.33	2.78	2.72	0.25	0.35

Specimens were cut out from the panels and the fibre volume fraction and void content were measured using the acid digestion method [16]. Typical values of 53% and 1% for the fibre volume fraction and void content, respectively were obtained. It has been noticed that the values between the resin inlet region and resin outlet region are quite similar for the fibre volume fraction however; the void content values in the outlet region are higher than the inlet region. This fact may be attributed to the vacuum gradient within the bag which is higher in the outlet than the inlet therefore reducing the void content in that region. In order to predict the laminate tensile strengths in the warp and weft direction, a simple rule of mixtures [1] was used and a typical value for the shear strength from unidirectional materials was used. The strengths and material parameters required for the model are summarised in Table 5. The predicted stress-strain curves for the warp, weft and inplane shear directions using the present damage model are shown in Fig. 5.

Table 5. Predictions for the laminate strengths[1] and material parameters

S_{11} (MPa)	S_{22} (MPa)	S_{12} (MPa)	ε_{11}^{0} (%)	ε_{22}^{0} (%)	ε_{12}^{0} (%)	ε_{11}^{f} (%)	ε_{22}^{f} (%)	α	n
2484	66	100	2.13	5.35	0.04	2.34	5.90	1.0	2.0

(1) Based on 53% of fibre volume fraction

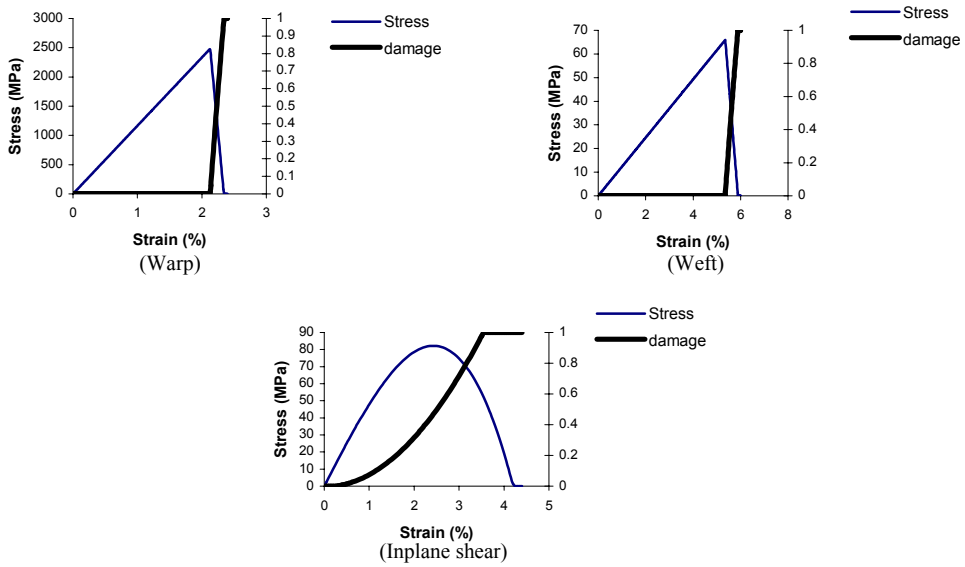

Fig. 5. Predicted stress-strain responses using the present damage model.

Fig. 6 shows a comparison between numerical predictions using the present damage model, existing Chang-Chang failure criteria [17] and experimental results.

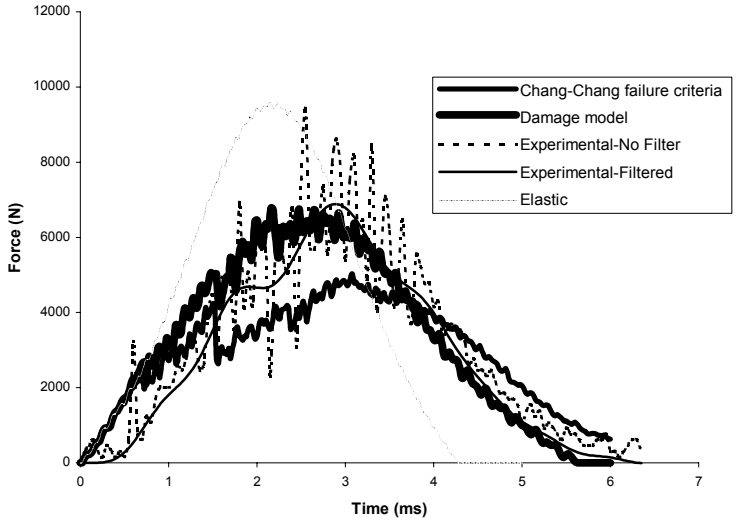

Fig. 6. Force history for impact energy of 20 Joules.

As shown in Fig. 6 the impact response predicted by the in-plane damage model correlates well the impact response obtained experimentally. Also, the initial stiffness during the elastic phase, which was predicted using the 3-D micromechanical model, was predicted reasonably well. For the composite specimen and impact energy studied in this work, the predominant failure mechanisms experimentally observed were delamination, matrix cracking and fibre breakage on the back face of the panel due to high bending stresses. The predicted damage pattern associated with the inplane failure is shown in Fig.7 and it correlates very well with the damage pattern observed experimentally. The performance of the damage model was also checked against the existing Chang-Chang failure criteria [17]. It can be seen from Fig. 6 that the Chang-Chang failure criteria underestimates the peak force as well as overestimating the impact duration.

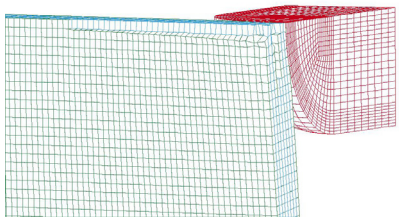

Fig. 7. Damage pattern due to tensile stresses on the back face of the laminate.

6. CONCLUSIONS

Manufacturing and modelling aspects for composite materials manufactured using RIFT process have been presented and discussed in this paper. Good quality panels with void contents around 1% have been manufactured using the proposed manufacturing methodology. The composites manufactured using the RIFT process described here were virtually tested using both a 3-D micromechanical analytical model and an in-plane failure model presented in this paper. Impact tests were undertaken in order to assess the reliability of the approach. The current damage model was able to predict the observed failure with good accuracy.

ACKNOWLEDGEMENTS

The authors acknowledge the financial support received for this work from the Brazilian National Research Council (CNPq), process 200863/00-2 (NV) and Mr. Akash Patel and Mr. Leon Yeung for helping to manufacture the composite plates and performing the impact tests.

REFERENCES

1. **Jones, M. R.**, "Mechanics of composite materials", *Taylor and Francis Inc.*, 2nd edition (1999).
2. **Ianucci L., Willows M., Dechaene R.**, "A failure model for the analysis of thin woven glass composite structures under impact loads", *Computer and Structures.*, **79** (2001), 785-799.
3. **Ianucci L.,** "Progressive failure modelling of woven carbon composite under impact", *Submitted to Int. J. Impact. Eng.*, (2004).
4. **Product Data Sheet,** *SP Systems Inc.* (2004)
5. **Chamis, C.C.**, "Simplified composite micromechanics equations for hygral, thermal and mechanical properties", *SAMPE Quarterly.*, **15**/3 (1984), 14-23.
6. **Kowalski, I. M.**, "Determining the transverse modulus of carbon fibres", *SAMPE Journal* **17,** (1986), 38-42.
7. **Torayca Carbon Fibre Data Sheets,** *Torayca Inc.* (2003).
8. **PPG Glass Fibre Data Sheets,** *PPG Industries Corporate.* (2004).
9. **Advanced Composite Compression Tests,** *Boeing Specification Support Standard,* BSS 7260 (1986).
10. **Naik, N.K.** and **Shembekar, P.S.**, "Elastic behaviour of woven composites-II: Laminate Analysis", *Journal of Composite Materials.*, **26**/15 (1992), 505-517.
11. **Chaboche, J.L.**, "Continuum damage mechanics I – General concepts", *J. Appl. Mech.*, **55**/1 (1988), 59-64.
12. **Taylor R. L., Matzenmiller A. Lubliner J.**, "A constitutive model for anisotropic damage in fibre composites", *Mechanics of materials,* **20**/2 (1995), 125-152.
13. **LS-DYNA 970.**, *Livermore software technology corporation ,* USA, (2003).
14. **Stillman D. W., Hallquist J.O.**, "Ingrid: A three-dimensional mesh generator for modelling non-linear systems", *University of California, Lawrence Livermore National Laboratory*, (1985).
15. **LS-PRE/POST v1.0.**, *Livermore software technology corporation ,* USA, (2003).
16. **British Aerospace**, *Test method for the fibre and void content measurements of cured carbon and glass fibre composites,* **3** (BAER 3014) (1990), 1-5.
17. **Chang F.K, Chang K.Y.**, "A Progressive Damage Model for Laminated Composites Containing Stress Concentration", *Journal of Composite Materials,* **21** (1987), 834-855.